Flexibility and Plasticity of Human Centrin 2 Binding to the Xeroderma Pigmentosum Group C Protein (XPC) from Nuclear Excision Repair[†,‡]

Ao Yang,[§] Simona Miron,[§] Liliane Mouawad, Patricia Duchambon, Yves Blouquit, and Constantin T. Craescu*

Integrative Imaging Unit, INSERM U759/Institut Curie-Recherche, Centre Universitaire Paris-Sud, Bâtiment 112, 91405 Orsay Cedex, France

Received December 6, 2005; Revised Manuscript Received January 25, 2006

ABSTRACT: Human centrin 2 is a component of the nucleotide excision repair system, as a subunit of the heterotrimer including xeroderma pigmentosum group C protein (XPC) and hHR23B. The C-terminal domain of centrin (C-HsCen2) binds strongly a peptide from the XPC protein (P1-XPC: $N_{847}-R_{863}$). Here, we characterize the solution Ca^{2+}-dependent structural and molecular features of the C-HsCen2 in complex with P1-XPC, mainly using NMR spectroscopy and molecular modeling. The N-terminal half of the peptide, organized as an α helix is anchored into a deep hydrophobic cavity of the protein, because of three bulky hydrophobic residues in position 1−4−8 and electrostatic contacts with the centrin helix E. Investigation of the whole centrin interactions shows that the N-terminal domain of the protein is not involved in the complex formation and is structurally independent from the peptide-bound C-terminal domain. The complex may exist in three different binding conformations corresponding to zero, one, and two Ca^{2+}-bound states, which may exchange with various rates and have distinct structural stability. The various features of the intermolecular interaction presented here constitute a centrin-specific mode for the target binding.

Centrins are small Ca^{2+}-binding proteins of the calmodulin (CaM)[1] superfamily, highly conserved in the eukaryote cells from yeast to humans. There are three human centrin isoforms (HsCen1−HsCen3), each having four potential Ca^{2+}-binding sites but different physicochemical and binding properties (*1*−*3*). Centrins were initially identified in the unicellular green algae, such as *Tetraselmis striata* (*4*) and *Chlamydomonas reinhardtii* (*5*), as major components of several types of Ca^{2+}-sensitive contractile fibers, including the nuclear-basal body connectors and the distal striated fibers. Later, homologous proteins were observed in the microtubule-organizing centers (MTOCs), named centrosomes in higher organisms and the spindle pole body (SPB) in yeast. MTOCs have a major role in nucleating and orienting the microtubule network, in particular during the formation of the mitotic spindle. It was shown that the duplication and segregation of centrosomes (or SPB) are critically dependent upon centrins in yeasts (*6*), algae (*7*), and human cells (*8*). Elucidation of the detailed mechanism of this function is only at the beginning, but accumulating evidence shows that the centrosomal role requires interactions with other protein targets (*9*, *10*). One of the first centrin/target interactions was described in the yeast SPB, where Cdc31p (the *Saccharomyces cerevisiae* centrin) can bind to a nuclear membrane protein of the half bridge, named Kar1p, with a dissociation constant of 60 nM (*11*). Another centrin target, named Sfi1, including a series of conserved repetitive motifs, was recently identified in the yeast SPB but also in the centrosomes of higher eukaryotes (*10*). Centrins, similar to other centrosomal proteins, are phosphorylated only during mitosis, but in some tumors, phosphocentrin may form at an inappropriate time during the cell cycle and accumulates in the centrosomes (*12*). Recent data with HeLa-cultured cells (*13*) suggested that the phosphorylation site is the Ser170, situated in a highly flexible C-terminal fragment of the protein.

As for CaM during the last 3 decades (*14*), new functional roles of centrins in various cell compartments are currently emerging from genetic, biochemical, and cell biology experiments. The centrosomal fraction of centrins was estimated as low as 10% (*15*), meaning that the majority of the protein is localized in other organelles, where it may play distinct roles. Indeed, two new functions, localized in the nucleus area, were recently identified, one related to the nucleotide excision repair (NER) system, through the interaction with

[†] This work was supported by the Centre National de la Recherche Scientifique, the Institut National de la Santé et de la Recherche Médicale, and the Institut Curie.

[‡] The atomic coordinates of an ensemble of 20 structures corresponding to the complex C-HsCen2/P1-XPC (code 2A4J) have been deposited in the Protein Data Bank (http://www.rcsb.org). The ^{1}H, ^{15}N, and ^{13}C chemical-shift values of this complex have been deposited in BioMagResBank (http://www.bmrb.wisc.edu) under the accession number 5992.

* To whom correspondence should be addressed: Integrative Imaging Unit, INSERM/Institut Curie-Recherche, Centre Universitaire Paris-Sud, Bâtiment 112, 91405 Orsay Cedex, France. Telephone: 33-1-69-86-31-63. Fax: 33-1-69-07-53-27. E-mail: Gil.Craescu@curie.u-psud.fr.

[§] These authors contributed equally to the work.

[1] Abbreviations: CaM, calmodulin; CrCen, *Chlamydomonas reinhardtii* centrin; HsCen1−HsCen3, human centrin 1−3; C-HsCen2, C-terminal domain of human centrin 2 (residues 94−172); N-HsCen2, N-terminal domain of human centrin 2 (residues 1−98); ITC, isothermal titration calorimetry; HSQC, heteronuclear single-quantum coherence; MD, molecular dynamics; MTOC, microtubule-organizing center; NER, nucleotide excision repair; SPB, spindle pole body; XPC, xeroderma pigmentosum group C protein.

10.1021/bi0524868 CCC: $33.50
Published on Web 02/28/2006

the heterodimer XPC/hHR23B (*16*), and another one in the mRNA export process, probably involving two partner proteins, Sac3 and Sus1 (*17*). Other possible functions were also suggested in the regulation of the G-protein transducin (G_t) in mammalian photoreceptor cells (*18*) or in the activity of the paramecium ciliary reversal-coupled voltage-gated Ca^{2+} channels (*19*).

Understanding of the centrin various cell functions, including target specificity, Ca^{2+} dependence, and interaction mode requires a detailed molecular and structural characterization of the protein in isolation and in physiologically relevant complexes. The structure determination of isolated centrins is hampered by its high structural flexibility and the tendency to self-associate (*20*). Using protein constructs covering separated domains of HsCen2, we were able to determine the solution structure of the N-terminal domain (*21*) and of a C-terminal construct including the D helix, which normally belongs to the N-terminal lobe (*2*). In this last structure, the Ca^{2+}-bound C-terminal domain assumes an open tertiary conformation, which binds the D helix in a mode evoking the interaction of CaM with target peptides (*14*).

NER is a major pathway for recognition and removal of bulky DNA single-strand lesions such as the UV-induced photoproducts or carcinogenic adducts. Its dysfunction produces severe disorders in humans, including xeroderma pigmentosum, a hereditary disease characterized by a high photosensitivity and a 10 000-fold increase of sunlight-induced skin cancers. One of the molecular components involved in several pathologic forms is the xeroderma pigmentosum group C protein (XPC) complex, a heterodimer composed of XPC and hHR23B, the human homologue of yeast Rad23B. The available experimental data suggest strongly that the XPC complex plays a key role in the initial phase of the Global Genome NER, consisting in the recognition of the damaged DNA and recruiting of other components of the repair pathway (*22*, *23*). The first indication on a possible role of centrins in the NER process was obtained from biochemical experiments (*16*), demonstrating that HsCen2 co-purifies with the complex XPC/hHR23B from HeLa nuclear extracts. Together with hHR23B, centrin seems to stabilize XPC through a direct physical interaction (*16*). Moreover, the interaction between HsCen2 and XPC plays a direct stimulatory role in the NER process, by enhancing the damage-specific DNA binding of the heterotrimer (HsCen2/XPC/hHR23B) (*24*). Recent studies using an *Arabidopsis* variant (*25*), confirmed and extended the hypothesis of the centrin functional role in the repair process, by showing that a low expression of the plant centrin is associated to a decreased NER activity, which in turn enhanced the homologous recombination.

Starting from the hypothesis of a direct physical interaction between HsCen2 and XPC, we identified a high-affinity centrin-binding site in the C-terminal part of XPC and characterized the interaction between a 17-residue peptide (P1-XPC: $N_{847}-R_{863}$), representing this site, and HsCen2 (*26*) (Figure 1). The binding has an affinity of 2.2×10^8 M^{-1} in the presence of Ca^{2+}, which is moderately decreased in the absence of the divalent cation (by a factor of 27) and essentially contributed by the C-terminal half of the centrin (C-HsCen2). The localization of the centrin-binding site was recently confirmed by using various human XPC constructs and binding assays (*24*).

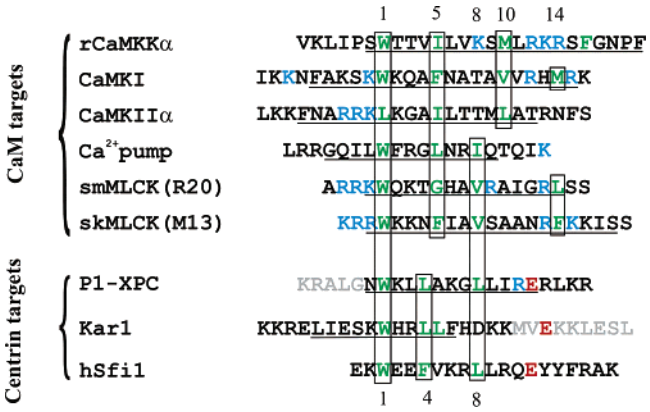

FIGURE 1: Sequences and motifs of CaM and centrin-binding peptides. Green residues indicate the bulky hydrophobic side chains anchoring the peptide into the hydrophobic pocket of the protein. They define the common patterns for the CaM (top) or centrin (bottom) targets. The peptide fragments forming a persistent structure in the complex are underlined. Blue (basic) and red (acidic) residues are involved in electrostatic interactions with the protein. Residues shown in gray represent portions of the target sequences that were not used in the structural or binding studies. Note that the sequence of the repeat in hSfi1 (residues 112−131) is reversed. References on the CaM target peptides are rCaMKKα (*55*), CaMKI (*56*), CaMKIIα (*35*), Ca^{2+} pump (*36*), smMLCK (R20), (*34*), and skMLCK (M13) (*33*).

Here, we present the NMR solution structure of the 1:1 complex formed by Ca^{2+}-saturated C-HsCen2 and the peptide P1-XPC. The N-terminal half of the peptide lies on the exposed deep hydrophobic cleft formed by the two open EF-hands of centrin and shows hydrophobic and electrostatic contacts with the side chains of the protein. NMR and MD simulations, applied to the peptide binding by the Ca^{2+}-saturated whole protein, suggest that the N-terminal half of the protein has a large structural independence and plays no role in the interaction with P1-XPC. The present results constitute the first atomic structure of a biologically relevant complex of human centrins and provide a useful molecular and energetic basis for the understanding of the first steps of the repair function.

MATERIALS AND METHODS

Protein Expression and Purification. The recombinant integral protein and its C-terminal domain ($T_{94}-Y_{172}$) were overexpressed in *Escherichia coli* as described previously (*1*, *2*). Purification used three chromatographic steps, including DEAE-TSK, phenyl-TSK, and G25 columns (*21*). Uniform ^{15}N and $^{15}N/^{13}C$ labeling were obtained using a minimal medium culture (M9) containing $^{15}NH_4Cl$ and ^{13}C-glucose as the sole source of nitrogen and carbon, respectively. The induction step (with 0.1 mM IPTG) was prolonged to 18 h in this case. The P1-XPC peptide with the sequence NWKLLAKGLLIRERLKR, derived from the human XPC protein ($N_{847}-R_{863}$), was purchased from Biofidal (Vaulx-en-Velin, France). The high-pressure liquid chromatography analysis indicated a purity greater than 95%.

C-HsCen2 Phosphorylation. The C-terminal domain (10 mg) was phosphorylated *in vitro*, using 4 μL of protein kinase A (5 megaunits/mg), 200 μL of ATP (2 mM), and 10 μL of NaN_3 (0.2%) in 50 mM Tris-HCl and 10 mM $MgCl_2$ (pH 7.5) at 30 °C. Evolution of the phosphorylation was followed by chromatography on CM-Trisacryl and SDS−PAGE (see

Figure S1 in the Supporting Information). After 76 h, analysis by mass spectrometry indicated that 95% of the protein was modified, and the samples were only desalted through a G25 gel filtration.

Ca^{2+} Titration. The protein samples, lyophilized after an extensive dialysis against ammonium bicarbonate buffer, usually contain 8−10% (mol/mol) Ca^{2+} contaminant. C-HsCen2 was dissolved in a Tris d_{11} (20 mM) buffer at pH 6.7, containing 200 mM NaCl, and the Ca^{2+} load was checked using 1D and heteronuclear single-quantum coherence (HSQC) spectra, while adding an increasing amount of buffered EDTA. At 6 mM EDTA, the fraction of the metal-bound protein is negligible (see Figure S2 in the Supporting Information). The peptide P1-XPC was added to this apo form, and Ca^{2+} titration of the complex was performed by adding small aliquots of a stock solution of $CaCl_2$ (0.35 M).

NMR Spectroscopy. NMR samples at the 0.6−1.2 mM concentration (pH 6.7) were obtained by dissolving the lyophilized protein in a buffer containing 20 mM deuterated Tris/DCl, 100−200 mM NaCl, and 5−10 mM $CaCl_2$, in 93% ^1H_2O/7% ^2H_2O or in 100% ^2H_2O. The unlabeled P1-XPC peptide was added in a slight molar excess. Two-dimensional homonuclear, as well as double- and triple-resonance (HSQC, NOESY−HSQC, TOCSY−HSQC, HNCA and HN(CO)CA, and HCCH−TOCSY) NMR experiments (*27*, *28*) were performed on Varian Unity-500 NMR and Bruker Avance-800 spectrometers at 308 K. Proton chemical shifts in parts per million (ppm) were referenced relative to internal DSS, while ^{15}N and ^{13}C references were set indirectly relative to DSS using frequency ratios (*29*). The NMR data were processed and analyzed using Felix software (Accelrys, San Diego, CA), running on Silicon Graphics Indigo workstations. For the 3D ^{15}N TOCSY−HSQC and NOESY−HSQC spectra, the data were extended by linear prediction in the indirect dimensions, zero-filled, and multiplied by sine-bell functions shifted by $\pi/4$ before Fourier transformation. The (^1H and ^{15}N) three-dimensional spectra were acquired with 7000 and 1500 Hz spectral width for ^1H and ^{15}N dimensions, respectively. A total of 128 complex points in the t_1 dimension (^1H), 32 complex points in the t_2 (^{15}N) dimension, and 2048 complex points in the acquisition t_3 dimension were collected.

Structure Calculation. The NOE restraints were classified in three classes: strong (1.8−3.0 Å), medium (3.0−3.8 Å), and weak (3.8−5.0 Å). Moreover, the NOE restraints in secondary-structure elements were imposed to fall into the standard ranges for helical segments [3.3−3.7 Å for $d_{\alpha N}(i,i+1)$, 4.2−4.6 Å for $d_{\alpha N}(i,i+2)$, 4.0−4.4 Å for $d_{NN}(i,i+2)$, and 2.6−3.0 Å for $d_{NN}(i,i+1)$] and for the β-strand structures [2.0−2.4 Å for $d_{\alpha N}(i,i+1)$]. A number of hydrogen bonds involved in the secondary-structural regions were also included as distance restraints by using an upper and lower distance of 2.2 and 1.8 Å for the H−O pairs and 3.3 and 2.7 Å for the N−O pairs. For α helices and β strands, the dihedral angle values of $\Phi_H = -60$ (±30°), $\Psi_H = -30$ (±40°), and $\Phi_S = -130$ (±30°), and $\Psi_S = 145$ (±35°) were used. The structure determination was performed using 1382 NOE intraprotein restraints (556 intraresidue, 303 sequential, 292 medium range, and 231 long range) and 73 intermolecular distance restraints (Table 1). Additional 84 restraints were derived from hydrogen-bond identification, and 121 dihedral restraints resulted from the secondary-structure determination. The calculation of the structures was done using the Discover software and the cvff force field (Accelrys, San Diego, CA) running on a SGI workstation. Starting from an initial extended conformation, 200 structures were generated using a simulated annealing approach, including a 30 ps high-temperature phase (at 1000 K), followed by a cooling phase (down to 300 K) of 8 ps, and final energy minimizations. A force constant of 20 kcal mol^{-1} Å^{-2} was used for NOE distance restraints. Φ and Ψ dihedral angle restraints were applied with a force constant of 30 kcal mol^{-1} deg^{-2}. The quality of the 20 final structures, selected according to the potential energy and the compatibility with experimental restraints, was analyzed using InsightII and PROCHECK−NMR programs.

Table 1: Restraint and Structural Statistics for the 20 Best Solution Structures of the C-HsCen2/P1-XPC Complex

restraint statistics		
intramolecular NOE restraints	1382	
intraresidue	556	40%
sequential	303	22%
medium range ($2 \le \|i-j\| < 5$)	292	21%
long range ($\|i-j\| \ge 5$)	231	17%
hydrogen-bond restraints	84	
dihedral-angle restraints (Φ,Ψ)	121	
intermolecular NOE restraints	73	
average number of restraint violations		
violations per structure (>0.5 Å)	none	
dihedral angle restraint violations (>10°)	none	
rmsd for covalent bonds relative to standard (Å)	0.024	
rmsd for covalent angles relative to standard (deg)	2.7	
average rmsd (Å) from the average structure		
helices E, F, G, H and β sheet[a]	0.35	
helices E, F, G, H and β sheet, peptide W2−L9[a]	0.38	
all atoms	3.33	
all atoms, only residues 100−167 and peptide W2−L9	1.41	
ensemble Ramachandran plot		
residues in the most-favored region (%)	81.4	
residues in additional allowed regions (%)	14.0	
residues in generously allowed regions (%)	3.3	
residues in disallowed regions (%)	1.3	

[a] Backbone atoms (N, C′, and Cα).

Molecular Dynamics (MD) Simulations of the Complex Formed by the Integral Protein. A model of the complex formed by the integral protein with P1-XPC was built using the coordinates of the Ca^{2+}-free N-terminal domain (*21*) and of the Ca^{2+}-bound C-terminal domain in complex with P1-XPC (this paper). The D and E helices, considered to be collinear (an extended model), were linked by the flexible fragment S98−K100. We started with four conformers in which the phase between the N- and C-terminal domains were fixed at 0°, 90°, 180°, and 270° (the phase is the dihedral angle between the normals from the mass center of each domain to the connecting helix direction as in Figure 4A). The energy was minimized first by fixing the backbone and relaxing the side chains and then by relaxing the whole system. These relaxations were made by minimizing the energy under harmonic constraints (not to confound with NOE restraints) to keep the structure close to its original conformation, with a decreasing force constant every 100 steps, from 100, to 50, 25, 10, and 5 kcal mol^{-1} Å^{-2} and finally 2000 steps without constraints. The obtained structures were then submitted to MD simulations at 300 K in the vacuum using the CHARMM program (*30*) and the explicit

hydrogen CHARMM22 force field (*31*). The protocol consisted of 6 ps of heating phase and 50 ps of equilibration phase under a total of 2620 distance (NOE) restraints, collected from the spectra of the integral protein/peptide complex, followed by 10 ps without restraints. A total of 20 trajectories were calculated starting from each of the four minimized structures, differing only by the assignment of their initial velocities. The Shake algorithm was used to maintain the bonds that involve a hydrogen atom, and the time step was 1 fs. The switch function was applied to the nonbonded interactions between 11 and 15 Å, and the dielectric constant was equal to 2*r*, with *r* being the distance between atoms.

Isothermal Titration Calorimetry (ITC). Thermodynamic parameters of molecular interactions between centrin and target peptides at 30 °C were investigated by ITC using a MicroCal MCS instrument (MicroCal, Inc., Northampton, MA). The proteins and peptides were equilibrated in the same buffer containing 50 mM MOPS at pH 7.4, 100 mM NaCl, and Ca^{2+} (1 mM). The protein (20 μM) in the 1.337 mL calorimeter cell was titrated by the peptide (generally 10 times more concentrated) by about 30 successive automatic injections of 7−10 μL each. The first injection of 2 μL was ignored in the final data analysis. Integration of the peaks corresponding to each injection and correction for the baseline were done using Origin-based software provided by the manufacturer. Fitting of the data to various interaction models gives the stoichiometry (*n*), equilibrium binding constant (K_a), and enthalpy of the complex formation (ΔH). Usually, control experiments, consisting of injecting peptide solutions into the buffer, were performed to evaluate the heat of dilution.

RESULTS

Structural Description of the C-HsCen2/P1-XPC Complex. The binding affinity of P1-XPC to HsCen2 was shown to be essentially due to the C-terminal domain of the protein and to increase moderately with the Ca^{2+} concentration (*26*). Therefore, we determined the structure of the C-HsCen2/P1-XPC complex under saturating Ca^{2+} concentrations, using NMR spectroscopy and MD methods. The small root-mean-square deviation (rmsd) values and the absence of any large constraint violations (Table 1) indicate a good quality for the final 20 structures. Analysis of the calculated structures by PROCHECK−NMR shows that more than 98% of the backbone dihedral angles are distributed in the allowed regions of the Ramchandran plot. A stereoview of the 20 best structures of the complex, superimposed on the backbone protein secondary structure elements, is represented in Figure 2A. The figure shows that C-HsCen2 in the complex adopts the classical structure of a Ca^{2+}-saturated EF-hand domain, with the two EF-hand motifs packed together through an antiparallel β strand. Local structural disorders, because of a lower (or the absence of) experimental restraint, may be noted in the N-terminal (94−99) and the C-terminal (168−172) ends of the domain, in the linker between the two EF-hand motifs, and in the four C-terminal residues of the peptide, while the α helices (E, K100−F113; F, F123−E132; G, D139−A149; H, E159−K167) and the β strands (β3, K120−S122; β4, E156−S158) are almost equally well-defined. The third Ca^{2+}-binding loop shows a less defined structure than the fourth loop, probably because of its

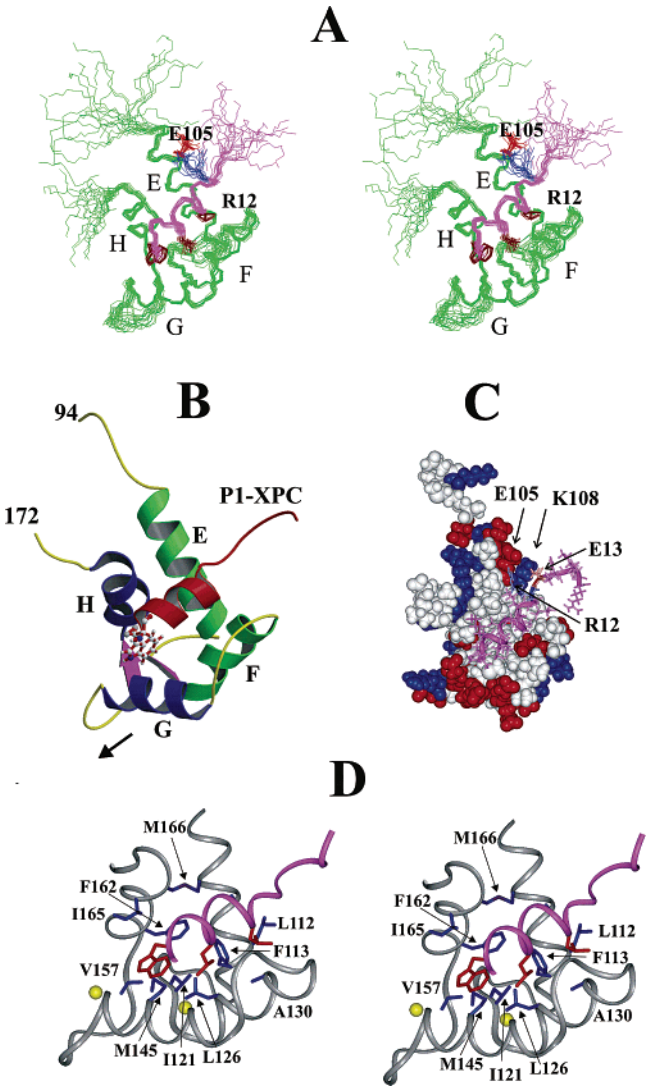

FIGURE 2: Structure of the complex formed by C-HsCen2 with the peptide P1-XPC in the presence of saturating Ca^{2+} concentrations. (A) Stereo representation of the superposition of the 20 best structures calculated by MD under NMR experimental restraints. The protein is colored in green, and the peptide is colored in magenta. The hydrophobic side chains of W2, L5, and L9 from the peptide are shown in brown. The electrostatic interaction between the peptide R12 (blue) and centrin E105 (red) residues results in the restricted conformational space explored by these residues, despite their exposure to the solvent. (B) Structure of the complex, represented with MOLSCRIPT (*57*) and Raster3D (*58*). The two EF-hands are colored in green and blue, while the peptide is red. The Trp residue of P1-XPC is the single side chain shown in this panel as a ball-and-stick model. The black arrow indicates the direction of the peptide displacement in the present complex relative to similar peptides in complex with CaM. (C) van der Waals surface of C-HsCen2 in complex with P1-XPC. Blue and red colors correspond to positively and negatively charged side chains, respectively. The ribbon representation of the peptide backbone and the side chains are shown in magenta, except for residues R12 and E13, which are colored in cyan and orange, respectively. The charged side chains of the protein contributing to the electrostatic interaction with the target are indicated by arrows. In the three panels, the molecular complex has similar orientations. (D) Stereoview of the complex with the main anchoring side chains of the peptide (red) and the principal protein residues involved in the interaction (blue). The backbone of the peptide (magenta) and the protein (gray) are shown in a ribbon representation. The position of the Ca^{2+} ions (yellow spheres) is approximately indicated, in analogy with the X-ray CaM structure (PDB 3cln).

Table 2: Thermodynamic Parameters of Various Peptides Binding to HsCen2 in the Presence of Ca^{2+}

protein	ligand	K_a (±error) (10^7 M^{-1})	ΔG (kcal/mol)	ΔH (±error) (kcal/mol)	$T\Delta S$ (kcal/mol)
HsCen2	P1-XPC	22 (4)	−11.6	−27.2 (0.2)	−15.6
C-HsCen2-Ph[a]	P1-XPC	7.1 (0.3)	−10.9	−29.0 (0.4)	−18.1
HsCen2	P1-XPC(W2A)	NB[b]			
HsCen2	P1-XPC(K3E)	9.2 (0.3)	−11.0	−30.2 (0.2)	−19.2

[a] Phosphorylated C-HsCen2. [b] NB = no binding observed in the present conditions ($<10^4$ M^{-1}).

significantly lower affinity for Ca^{2+} (*1*, *2*). The two EF-hands adopt an open conformation with the two α helices in an almost perpendicular arrangement (Figure 2B), creating a deep hydrophobic cavity, bordered mostly by negatively charged side chains (Figure 2C). The mean interhelical angles in the two EF-hand motifs, calculated with the Interhlx software (K. Yap, University of Toronto) are E/F = 112° and G/H = 103°, in the range of values observed for the majority of the regulatory EF-hand domains and particularly close to the solution structure of Ca^{2+}-bound CaM (*32*). These values are significantly different from those determined for the N-terminal domain of HsCen2 (151°, 141°), which does not bind calcium in physiological conditions and exhibits a closed conformation (*21*).

The peptide, which is highly disordered in the absence of the protein (*26*), folds into an α helix, spanning the fragment N1−L9. The helical portion is deeply embedded in the large hydrophobic pocket of C-HsCen2 and shows many contacts involving bulky hydrophobic side chains (Figure 2D), mainly W2, L5, and L9, which define the pattern 1−4−8 (numbering from W2 that can be noted W^1, see Figure 1). W2 of the peptide appears to be the most deeply buried in the hydrophobic pocket and shows the largest number of intermolecular NOE interactions. To assess the importance of this residue for the binding, we synthesized a mutant peptide (W2A) and measured its affinity by ITC. The binding to HsCen2 or C-HsCen2 was undetectable ($<10^3$ M^{-1}) in the same experimental conditions used for the wild type (Table 2), for which the binding constant is 2.2×10^8 M^{-1} (*26*). This result points to the critical role of the W2 residue and suggests an efficient way to block the HsCen2/XPC interaction in the cell context. A parallel experiment, using the peptide variant K3E (Table 2), showed a conserved binding affinity ($K_a = 9.2 \times 10^7$ M^{-1}), demonstrating that the positive charge on the peptide N side has no significant impact on the interaction energetics.

The last 5 C-terminal residues in C-HsCen2, including a biologically relevant phosphorylation site (S170) (*13*), are very flexible and show no unique structure (Figure 2A). To assay a possible role of the phosphoryl group in the XPC binding, we phosphorylated in vitro C-HsCen2 (using protein kinase A) and analyzed its molecular properties. Far-UV CD spectra of this modified domain showed no significant changes in the secondary-structure content relative to the wild-type form, both in the presence and absence of Ca^{2+} ions (see Figure S1 in the Supporting Information). Also, ITC experiments demonstrated that S170 phosphorylation does not change the affinity for P1-XPC (Table 2). These data suggest strongly that the phosphorylation of this site is not critical for the centrin interaction with XPC.

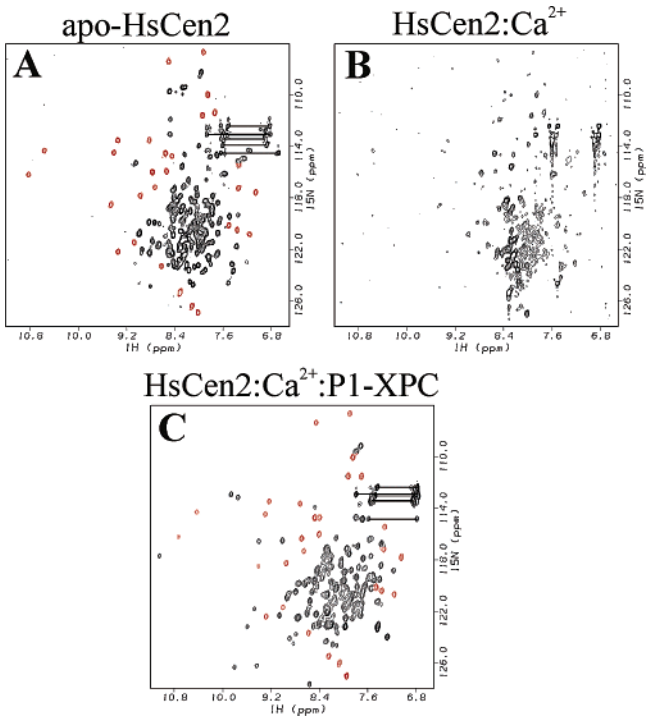

FIGURE 3: HSQC spectra of ^{15}N uniformly labeled centrin. (A) HsCen2 in the absence of Ca^{2+} and peptide, (B) in the presence of 1 equiv of Ca^{2+} but no peptide, and (C) in complex with an equimolar concentration of Ca^{2+} and P1-XPC. The protein is 1.5 mM in Tris d_{11} buffer at pH 6.7, and the spectra were recorded at 298 K. The red peaks in A and C represent the most shifted resonances assigned to the N-terminal domain, and the horizontal lines connect proton resonances of NH_2 groups.

The Centrin N-Terminal Domain Is Not Critically Involved in XPC Binding. As mentioned above, one of the main centrin-specific binding features is related to the dominant role played by the C-terminal domain of HsCen2. To check a possible role of the N-terminal domain, we analyzed the NMR spectra of the P1-XPC in complex with the integral centrin. In the peptide-free apoprotein (Figure 3A), the C-terminal half adopts a highly fluctuating molten-globule state, with a limited proton chemical-shift dispersion, while the N-terminal half shows largely shifted and narrow peaks, indicating a unique and regular fold. Moreover, a detailed analysis of the NMR spectra reveals a high similarity between the spectral features of the N-terminal domain alone or as a part of the integral protein, strongly suggesting that the structure of the domain is essentially conserved (*21*). Therefore, linking the two halves of the protein together maintains the conformational features of the folding units, consistent with a high structural autonomy.

In the presence of 1 equiv of Ca^{2+}, where the fourth metal-binding site should be saturated (*2*), the HSQC spectrum shows a severe line broadening (Figure 3B) that concerns the majority of the cross-peaks from both domains. This observation reflects the presence of large centrin self-assemblies (*20*) and illustrates the experimental difficulties for the NMR investigation of the metal-bound states. The addition of the peptide dissociates the large centrin aggregates, resulting in a more dispersed and better resolved spectrum (Figure 3C). The increased spectral dispersion originates from the large shift of the C-terminal resonances, because the signals corresponding to the N-terminal domain (red peaks in Figure 3C) show no significant perturbation.

Analysis of the NMR spectra of the Ca^{2+}-saturated protein/peptide complex indicates that the N-terminal domain of human centrin 2 (N-HsCen2) conserves the three-dimensional structure determined in the isolated form (*21*) and shows no contacts with the C-terminal domain or the peptide. In absence of a hydrophobic pocket, the N-terminal domain may only interact with other partners through its exposed surface, which includes a distinct hydrophobic patch surrounded by positive charges (*21*). It is worth noting that the linker connecting the two domains of the protein in the HsCen2/P1-XPC complex has a helical structure, with a disordered region of 3 residues between S98 and K100, a situation which is different from the CaM/peptide complexes where the disrupted helix spans over 8−11 residues (*33*−*36*). However, the flexibility of the central linker fragment denotes the presence of uncorrelated motions of the two lobes, resulting in multiple conformations, similarly to the case of CaM (*32*, *37*).

The Modeled Structure of the Integral Centrin in Complex with the XPC Peptide. To check whether one or several relative positions of the two domains are energetically favored, we undertook a MD exploration of the conformational space spanned by the HsCen2/P1-XPC complex, using the experimental NMR distance restraints. In these calculations, we are faced with the problem of the absence of experimental information permitting us to define the relative position of the two centrin domains. For this reason, four starting extended conformers were modeled from the structures of the C-HsCen2/P1-XPC complex and of N-HsCen2 (*21*), linked by an unconstrained linker of residues S98−K100. In constructing the initial structure of the entire protein, the last helix of the N domain (helix D) was put collinear to the first helix of the C domain (helix E), similar to their position in CaM. The junction between these two helices was constructed in four different ways by changing the relative position of the two domains: the N and C lobes were either in phase, i.e., on the same face of the longitudinal axis, in opposite phase, or orthogonal to each other (Figure 4A). Starting from these structures, the MD simulations under NMR distance restraints generated a family of 80 structures of the complex, 20 for each initial conformation. The superposition of the final structures, using the helices of the N domain, is shown in Figure 4B. While the structure of each domain is well-conserved during the trajectories, there is no preferred relative arrangement of the two halves of the protein, although some parts of the space seem to be rather prohibited. Indeed, we did not obtain any structure corresponding to the phase between 30° and 65° as it can be seen in Figure 4C. This is due to the fact that, in such conformations, the charged residues of helix H (K167 and K168) would face the positively charged residues (K65 and K66) of the EF-hand linker in the N domain. Moreover, the in-phase conformation of the protein (phase 0) appears to be incompatible with the collinearity of the D and E helices, because of the attraction between the two domains in this configuration. On the contrary, in the phase 270°, the structures could span from very extended to completely closed conformations (Figure 4D). In fact, only one globular conformation was observed in all calculations; it is energetically as favorable as the others, with the same number of restraint violations at 0.5 Å (an average of 45, for a force constant of only 10 kcal mol^{-1} $Å^{-2}$). It is worth noting that

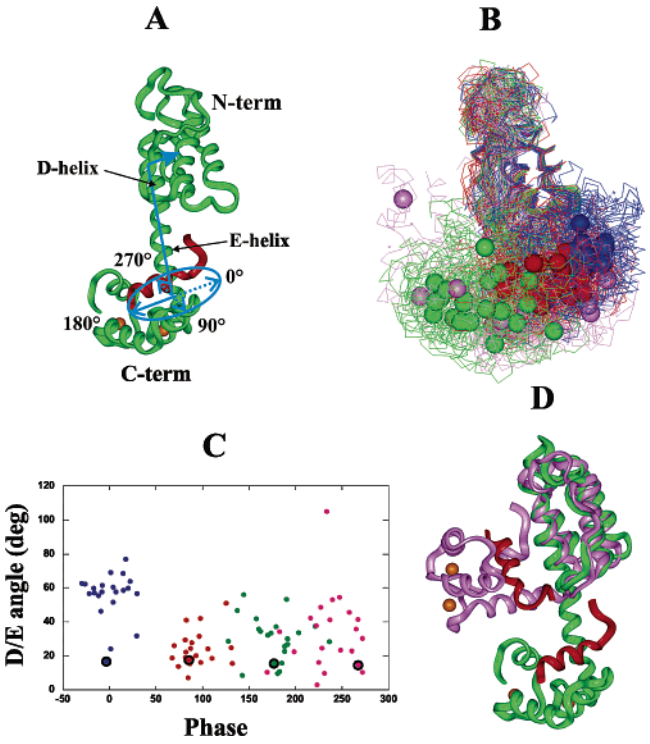

FIGURE 4: Molecular flexibility of the complex HsCen2/P1-XPC. (A) One of the four extended conformations of the HsCen2/P1-XPC complex of the integral protein used as initial structures for molecular modeling under NMR restraints. Calcium ions bound to the C-terminal sites are represented as orange spheres. The figure shows the antiphase conformer (phase = 180°) in which the mass centers of the two domains are on opposite sides of the central connecting helix (made of D and E helices). The blue axes define the phases of the four starting conformers. (B) Best superposition of the 80 final structures generated with the restrained MD calculations. The superposition was done using the heavy backbone atoms in regular structure elements of the N-terminal domain. The spheres represent the mass center position in the final structures obtained with in-phase (blue), anti-phase (green), and orthogonal (red and magenta) starting conformers. (C) Angle between helices E and D, reflecting the degree of bending of the structure, versus the phase between the two domains. Angle 0 corresponds to a well-extended structure, while the isolated point at 115° corresponds to the most closed structure. The color code is the same as in B. (D) Two final structures superimposed on the N-terminal domain, selected to illustrate the most extended (green) and the most bent (magenta) conformations of the complex.

this conformation does not have the shape of the globular CaM/peptide complexes because the N domain in HsCen2 could not open and engulf the ligand as in CaM (Figure 6).

One may ask whether there are conflicts between the NMR restraints and the CHARMM force field for some of the complex conformations. For this purpose, 10 ps of free dynamics were performed, starting from each of the 80 final structures obtained under restraints, solely to relax the system. They showed the same qualitative features as described above; i.e., the two halves of the protein adopt a wide variety of relative positions, going from the extended structures to the closed ones. This conformational space, explored by the HsCen2/P1-XPC is much larger than that explored by CaM in the study of Bertini et al. (*37*), because in the case of centrin, the closed form of the N domain allows for more accessible space to the C domain.

Ca^{2+}-Dependent Interaction Modes between C-HsCen2 and P1-XPC. As the centrin N-terminal domain is not

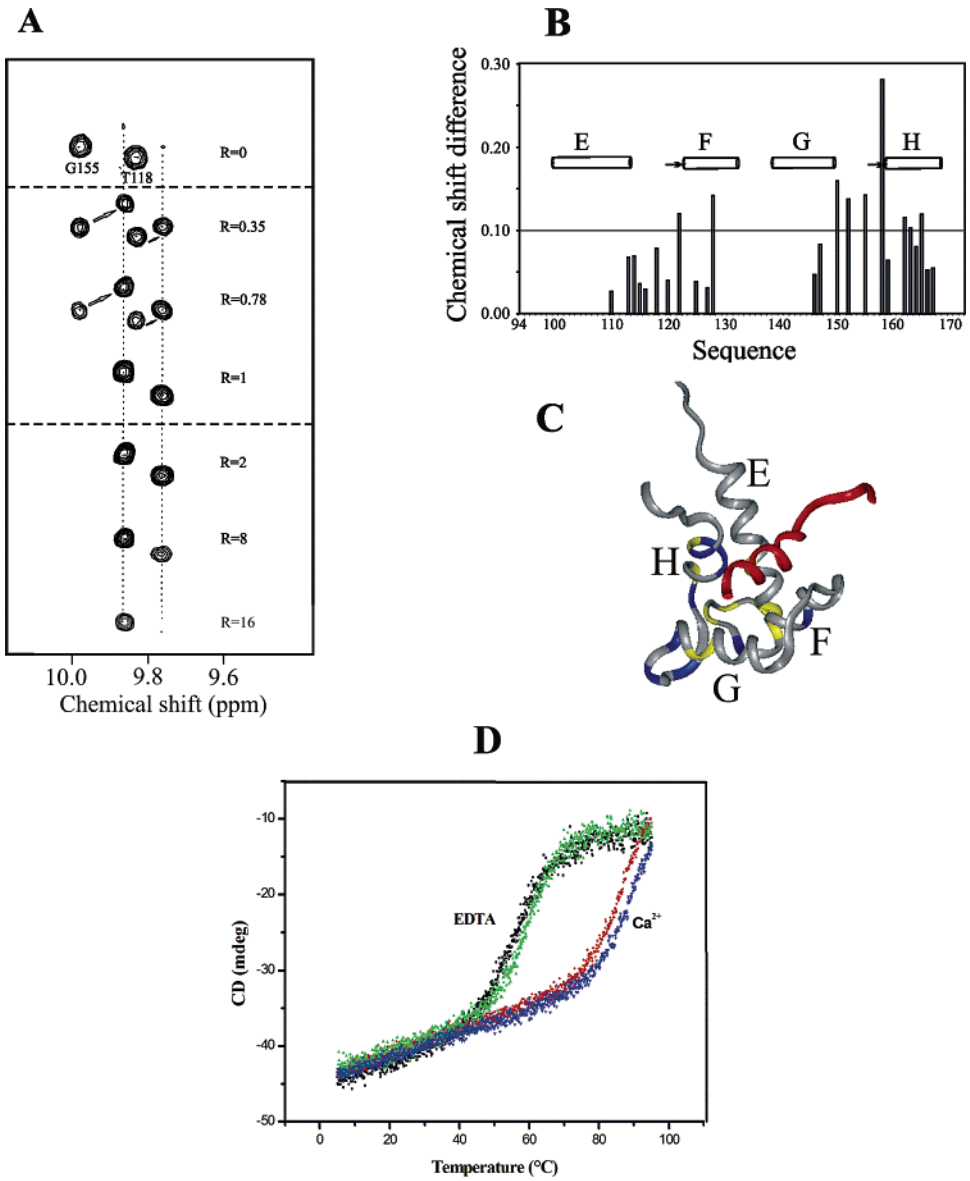

FIGURE 5: Ca^{2+} dependence of the interaction properties of C−HsCen2 and P1-XPC. (A) Evolution of the spectral area including T118 and G155 peaks during the Ca^{2+} titration, specified on the right side of the panel by the Ca^{2+}/protein ratio, *R*. (B) Distribution along the protein sequence of the composite chemical-shift distance (calculated as $\Delta\delta = \sqrt{[(\delta H)^2 + (\delta N/5)^2]}$), between the peaks corresponding to the zero and one Ca^{2+}-bound states of the complex. (C) Same values are represented on the ribbon structure of the complex, using blue and yellow colors for chemical-shift differences higher or lower than 0.1 ppm, respectively. The protein backbone is shown in gray, and the peptide is shown in red. (D) Thermal denaturation curves of C-HsCen2/P1-XPC complexes, obtained by monitoring the circular dichroism signal at 222 nm between 5 and 95 °C. Samples are 20 μM in Bis-Tris buffer (10 mM) at pH 7.2 and 25 mM NaCl. EDTA (5 mM) or $CaCl_2$ (2 mM) were used to ensure the apo- and metal-bound states, respectively. Black and red represent the native protein complex, while green and blue represent the phosphorylated (at S170) protein complex.

significantly engaged in the XPC binding, we focused on the C-terminal domain to study the Ca^{2+} dependence of the interaction. In the absence of Ca^{2+} and target peptide, C-HsCen2 shows the properties of a molten-globule state (*2*) with proton resonances confined to a narrow spectral range between 7.4 and 8.7 ppm (see Figure S2 in the Supporting Information). The addition of a slight excess of P1-XPC to the apo (^{15}N)C-HsCen2 induces important changes, resulting in a widely dispersed spectrum (a 3-fold larger proton spectral range) with sharp peaks, closely resembling that of the Ca^{2+}-saturated protein/peptide complex. This observation indicates that C-HsCen2 binds the peptide even in the absence of Ca^{2+} ions and forms a well-structured complex, consistent with the high value of the binding constant both in the presence and absence of metal ions (2.2×10^8 and 7×10^6 M^{-1}, respectively) (*26*). The considerable peptide-induced spectral changes should reflect important structural rearrangements and a decreased flexibility, as indicated by the large negative entropic contribution to the binding energy (*26*).

The Ca^{2+} titration of the protein/peptide complex is illustrated in Figure 5A through a HSQC spectral region, including one representative peak from each Ca^{2+}-binding loop, T118 (site III) and G155 (site IV). The substoichiometric ion concentration range is accompanied by a moderate chemical-shift change for about 25 amide peaks (including T118 and G155) with no line broadening. This means that the binding of the first metal ion to the high-affinity site

(IV) induces a new conformational state, which is in very slow exchange with the Ca^{2+}-free complex conformation. Parts B and C of Figure 5 show the mixed chemical-shift difference (^1H and ^{15}N) between the peaks of the two conformations, mapped onto the sequence and the three-dimensional structure. The spectral perturbations are mainly localized on the two calcium-binding loops but are significantly larger at the higher affinity site. They are also observed on the neighboring helices, especially F and H, which are in closer contact with the peptide. These observations suggest that the first binding step rearrange the fourth binding loop conformation but also affects the structure of the third site, probably via the structural link constituted by the intermotif EFβ scaffold (*38*). Structural coupling of the binding sites within EF-hand domains is often associated with a positive cooperativity for ion binding, with free-energy coupling of less than -2 kcal/mol (*39*). This feature was described for CaM (*40*) and other members of the EF-hand superfamily, such as calbindin D_{9k} (*41*) and *Nereis* sarcoplasmic calcium-binding protein (*42*). Lack of the intrinsic affinity value for site III, precludes a similar analysis of ion-binding cooperativity in the HsCen2/P1-XPC complex.

In the second titration step, the metal ion binds with a considerably lower affinity to the loop III. The spectral consequence consists of a gradual broadening of a few selected peaks in (or around) this binding loop (D116, T118, I121, and S122), while the chemical shift and line width of the remaining peaks are conserved (Figure 5A). At a high metal/protein ratio ($R = 16$), the broadened peaks completely disappear. These data are consistent with a progressive saturation of site III, which is in a fast-to-intermediate exchange between bound and free states. According to the chemical-shift perturbations, the Ca^{2+}-induced conformational changes are localized only to several residues of the binding loop III with minimal consequences on the rest of the protein domain.

The main conformational and dynamic changes, reflected in significant chemical-shift modifications and line narrowing, take place at the transition from the apoprotein to the C-HsCen2/P1-XPC complex. The effect of Ca^{2+} addition is essentially localized around the binding loops, suggesting that the metal ion produces minimal structural rearrangements of the apo complex that must be close to the structure determined in this paper (Figure 2). In contrast, Ca^{2+} binding considerably increases the structural stability of the complex, as reflected in the 25 °C shift of the mid-temperature of the thermal denaturation (Figure 5D). Stabilization of the metal-binding loops should decrease the standard free energy of the native state and reduce the amplitude of the conformational fluctuations, with minimal changes in the global fold. Thus, the Ca^{2+} titration experiments revealed three distinct interaction states (with 0, 1, and 2 Ca^{2+} bound) between C-HsCen2 and P1-XPC, characterized by different conformations and lifetimes (Figure 5A). This unusual plasticity and flexibility of centrins provide the molecular basis for a high versatility in the recognition of various targets and allow for a quick reversibility of the signaling events.

The quantitative measure of the Ca^{2+} affinity enhancement induced by the presence of the target peptide or of the increase in peptide binding in the presence of Ca^{2+} ions may be expressed as the free-energy coupling $\Delta\Delta G$ between the two interaction processes (*43*). From the Ca^{2+}-induced increase in peptide binding (*26*), we calculated $\Delta\Delta G = -2.0$ kcal/mol. As suggested by the analysis of the Ca^{2+} titration of the protein/peptide complex, binding of the first metal ion produces the main conformational change of the complex and therefore must play the main role in the enhancement of peptide affinity. From the energy-coupling relationship, we may estimate that peptide binding produces an increase of the site IV affinity by more than an order of magnitude. The direct biological consequence of this observation is that, in the cellular environment and in the presence of a strong target like XPC, the Ca^{2+} affinity of the strong site in centrins is on the order of 10^6 M^{-1}, comparable to that of CaM (*40*). It is interesting to note that a longer construct of C-HsCen2, in which the D helix is also added to the C-terminal half and occupies roughly the place of the target peptide, also shows an 18-fold increased Ca^{2+} affinity (*2*).

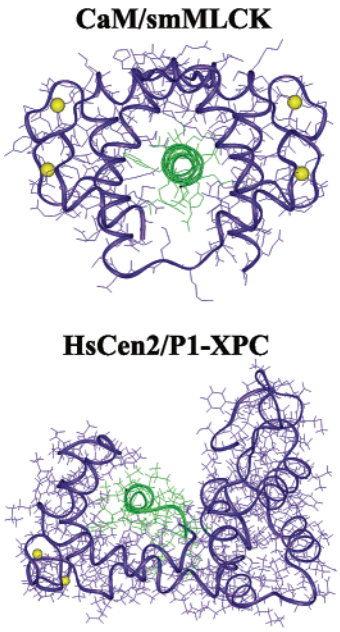

FIGURE 6: Comparison of the peptide-bound centrin and CaM structures. The structure of CaM in complex with the smMLCK peptide (PDB 1cdl) was determined by X-ray diffraction (*34*). HsCen2/P1-XPC is represented by the most compact structure from the 80 complex models generated with MD calculations under NMR restraints. In the two complexes, shown in similar orientations, the protein backbone and side chains are purple, the peptides are green, and the Ca^{2+} ions are yellow.

DISCUSSION

Specific Features of Centrin Interactions. The ensemble of the structural and molecular data obtained in this paper reveal an original interaction mode between HsCen2 and the peptide derived from the protein XPC. In most of the CaM/peptide complexes studied thus far (*44*, *45*), the two lobes of the protein show multiple atomic contacts with the peptide, which is engulfed in a hydrophobic channel formed by the two open EF-hand domains (Figure 6). The complex has a stable globular shape, with the central linker region unwound and bent by about 100° relative to the extended conformation observed in the Ca^{2+}/CaM crystal structure (*46*). Because of its incapacity to bind Ca^{2+} ions, the N-terminal domain of the human centrin 2 has a closed conformation and shows no significant interaction with the target peptide (Figure 6).

As in the solution structure of peptide-free CaM (*32*, *37*), the two lobes of the HsCen2/P1-XPC complex exhibit a stable conformation but their relative position is highly variable. The modeling under NMR restraints suggests a significant preference for elongated global shapes (Figure 4), but even in the most compact form, the protein/peptide interactions involve only the C-terminal domain of centrin (Figure 6).

The structural characteristics of CaM/peptide complexes revealed several interaction patterns based on the recognition of key hydrophobic residues along the peptide sequence, which may be accompanied by electrostatic attraction between charged side chains (*14*). The majority of CaM-binding peptides engage interactions with both CaM domains, with the N-terminal anchoring residue of the peptide (often a W) usually bound to the CaM C domain and another distant residue (in position 10, 14, or 16 relative to W^1) bound to the CaM N domain (*47*). At the interface with the C-terminal domain of CaM, peptide bulky hydrophobic side chains in position 1, 5, or 8 are the most important for binding. The results obtained in this paper suggest that a slightly different pattern, 1−4−8, may be characteristic for centrin-binding peptides. Indeed, in position 4, one usually observes only shorter side chains in CaM-binding peptides (Figure 1), while P1-XPC as well as Kar1 from the yeast SPB (*48*) exhibit a bulky hydrophobic residue. Another centrin target Sfi1 (*10*) shows multiple repeats with the same pattern, provided that the binding direction of the peptide is reversed (Figure 1).

The multiple interactions of the anchoring side chain in position 4 increase the binding energy of the centrin targets and possibly compensate for the lack of additional interactions with the N-terminal domain. Indeed, although contributed only by the C-terminal domain of centrin, the P1-XPC-binding free energy is comparable with that of the CaM/peptide complexes (*26*, *49*), in which both protein halves participate in the complex formation. The deep embedding of the residues L5 and L9 in the centrin pocket may be rationalized by the presence in centrins of a highly conserved Ala residue (A130 in HsCen2) in place of a flexible but much larger Met residue in CaM (M109), allowing for a larger hydrophobic cavity. A comparison of the present complex structure with available CaM complexes shows indeed that the P1-XPC is slightly axially shifted in the N-terminal direction (Figure 2B), permitting a deeper embedding of the bulky peptide side chains in the available space.

In the peptide, the fragment situated right after the α helix, including residues L10, I11, R12, and E13, shows an irregular but well-defined structure, as may be seen from the good superposition of its backbone in the structural ensemble (Figure 2A). Because no NOE interactions were observed in the NMR spectra, the position of this fragment is probably defined by the electrostatic interactions between the pair of complementary charged side chains of the peptide/protein residues (R12/E105 and E13/K108) allowed by the force field of the MD procedure. A closer inspection of the structural ensemble of the complex shows that the side chains of the pair R12/E105 are in close contact and exhibit a better superposition than the neighboring pair (E13/K108) (parts A and C of Figure 2). The charge interactions involving E105 have a correspondence in many CaM (E84) complexes with peptide targets, where they are thought to be particularly important for maintaining the bend of the interdomain linker (*34*). In contrast, the positively charged K108 corresponds to a Glu side chain in CaM (E87), where it interacts with basic residues of the target peptide (*33*, *50*). The electrostatic interactions involving the K108 side chain of centrins may accommodate the presence of a negatively charged residue in the C terminus of target peptides (Figure 1) and constitute another specific feature of the centrin-binding selectivity. Thus, in the absence of an anchoring interaction within the hydrophobic cavity from the N half of centrin, the target peptide adapts its structure and position to optimize the hydrophobic and electrostatic interactions with the C-terminal residues.

The functional relevance of electrostatic interactions in centrins was first emphasized by the discovery of a *C. reinhardtii* phenotype (vfl2) (*7*), where the *C. reinhardtii* centrin (CrCen) mutation E101K (equivalent to E105K in HsCen2) induces perturbations in the localization of the basal bodies and/or their segregation. In light of the present data, the molecular mechanism of this phenotype may be explained by a decreased affinity for a specific molecular partner necessary for the assembly of filamentous structures in the basal body. More recently (*51*), the mutation E → G in the equivalent position of the yeast Cdc31p was shown to give a temperature-sensitive phenotype, considered to be due to alterations of distinct functions of the centrin.

Biological Implications. Accumulating evidence shows that the physical interaction between HsCen2 and XPC is relevant for the efficiency of DNA repair through nucleotide excision (*16*, *24*, *25*), particularly by increasing the DNA-binding affinity and the discrimination capacity between nondamaged and damaged molecules in the first steps of the process (*24*). The present data constitute a first insight into the structural and molecular mechanism of this centrin function.

The capacity of HsCen2 to bind strongly P1-XPC even in the absence of Ca^{2+} means that in conditions of very low cell calcium concentrations centrin may be stably coupled to XPC, as a constitutive component of the damaged DNA-binding complex. Although not involved directly in the interaction with the binding site studied here, the N-terminal domain of the XPC-bound centrin may engage in interactions with (and modulate the structure of) other regions of the XPC/hHR23B complex. In contrast with other EF-hand domains, N-HsCen2 lost the metal-binding capacity and keeps a closed fold in physiological conditions. However, its uncommon basic character and the presence of several hydrophobic patches (*21*) allow for interactions with nonpolar or acidic sites in the heterotrimer.

At low cell Ca^{2+} concentrations, binding of only one metal ion to the fourth site of centrin strengthens the preformed complex and considerably limits its molecular flexibility, as reflected in the large increase of the thermal stability (Figure 5D). This dramatic change in the complex dynamics may modulate the DNA binding by increasing the specificity for the damaged sequences. In this proposed mechanism, calcium signaling triggers a reinforcement of the damage detection efficiency of the heterotrimer HsCen2/XPC/hHR23B, through a dynamics-mediated process. Indeed, folding of some unstructured domains (*52*) and a decrease of the internal flexibility of proteins (*53*) often accompany the sequence-specific DNA binding. At higher ion concentrations, other Ca^{2+} sensor proteins such as CaM become activated and may compete (with distinct affinity) for common molecular

targets. The fact that HsCen2 requires only one bound Ca^{2+} for optimal target binding means that the NER centrin function is activated at lower metal concentrations, before the induction of many other CaM-signaling processes.

The centrin target peptide (P1-XPC) is situated in the C domain of XPC, which is also involved in the binding of the transcription factor IIH (*54*). The critical interaction between XPC and TFIIH is necessary for the successful continuation of the repair process. Experiments using reconstituted functional complexes (*16*) showed that the NER still works, albeit less efficiently, in the absence of HsCen2, suggesting that TFIIH could bind independently to the C-terminal domain of XPC. Proximity (or superposition) of the binding sites for centrin and the transcription factor renders improbable the simultaneous binding of the two proteins to XPC, suggesting a possible sequential mechanism. Additional experiments, both on reconstituted and cell systems, are necessary for an in-depth understanding of the physicochemical basis of the DNA damage recognition and repair through nucleotide exchange.

ACKNOWLEDGMENT

S. M. gratefully acknowledges the Marie-Curie postdoctoral fellowship from the European Community. We acknowledge the access to the NMR national facility of Gif-sur-Yvette.

SUPPORTING INFORMATION AVAILABLE

Figure S1, SDS−PAGE (13% acrylamide) of the C-HsCen2, indicating the progress of phosphorylation; Figure S2, Ca^{2+} titration of the complex formed by (^{15}N)C-HsCen2 and P1-XPC. This material is available free of charge via the Internet at http://pubs.acs.org.

REFERENCES

1. Durussel, I., Blouquit, Y., Middendorp, S., Craescu, C. T., and Cox, J. A. (2000) Cation- and peptide-binding properties of human centrin 2, *FEBS Lett. 472*, 208−212.
2. Matei, E., Miron, S., Blouquit, Y., Duchambon, P., Durussel, I., Cox, J. A., and Craescu, C. T. (2003) The C-terminal half of human centrin 2 behaves like a regulatory EF-hand domain, *Biochemistry 42*, 1439−1450.
3. Cox, J. A., Durussel, I., Firanescu, C., Blouquit, Y., Duchambon, P., and Craescu, C. T. (2005) Calcium and magnesium binding to human centrin 3 and interaction with target peptides, *Biochemistry 44*, 840−850.
4. Salisbury, J. L., Baron, A., Surek, B., and Melkonian, M. (1984) Striated flagellar roots: Isolation and partial characterization of a calcium-modulated contractile organelle, *J. Cell Biol. 99*, 962−970.
5. Huang, B., Mengersen, A., and Lee, V. D. (1988) Molecular cloning of cDNA for caltractin, a basal body-associated Ca^{2+}-binding protein: Homology in its protein sequence with calmodulin and the yeast CDC31 gene product, *J. Cell Biol. 107*, 133−140.
6. Paoletti, A., Bordes, N., Haddad, R., Schwartz, C. L., Chang, F., and Bornens, M. (2003) Fission yeast cdc31p is a component of the half-bridge and controls SPB duplication, *Mol. Biol. Cell 14*, 2793−2808.
7. Taillon, B. E., Adler, S. A., Suhan, J. P., and Jarvik, J. W. (1992) Mutational analysis of centrin: An EF-hand protein associated with three distinct contractile fibers in the basal body apparatus of *Chlamydomonas*, *J. Cell Biol. 119*, 1616−1624.
8. Salisbury, J. L., Suino, K. M., Busby, R., and Springett, M. (2002) Centrin-2 is required for centriole duplication in mammalian cells, *Curr. Biol. 12*, 1287−1292.
9. Vallen, E., Ho, W., Winey, M., and Rose, M. D. (1994) Genetic interactions between CDC31 and KAR1, two genes required for dupplication of the microtubule organizing center in *Saccharomyces cerevisiae*, *Genetics 137*, 407−422.
10. Kilmartin, J. V. (2003) Sfi1p has conserved centrin-binding sites and an essential function in budding yeast spindle body duplication, *J. Cell Biol. 162*, 1211−1221.
11. Baum, P., Furlong, C., and Byers, B. (1986) Yeast gene required for spindle pole body duplication: Homology of its product with Ca^{2+}-binding proteins, *Proc. Natl. Acad. Sci. U.S.A. 83*, 5512−5516.
12. Lingle, W. L., Lutz, W. H., Ingle, J. N., Maihle, N. J., and Salisbury, J. L. (1998) Centrosome hypertrophy in human breast tumors: Implications for genomic stability and cell polarity, *Proc. Natl. Acad. Sci. U.S.A. 95*, 2950−2955.
13. Lutz, W. H., Lingle, W. L., McCormick, D., Greenwood, T. M., and Salisbury, J. L. (2001) Phosphorylation of centrin during the cell cycle and its role in centriole separation preceding centrosome duplication, *J. Biol. Chem. 276*, 20774−20780.
14. Crivici, A., and Ikura, M. (1995) Molecular and structural basis of target recognition by calmodulin, *Annu. Rev. Biophys. Biomol. Struct. 24*, 85−116.
15. Paoletti, A., Moudjou, M., Paintrand, M., Salisbury, J. L., and Bornens, M. (1996) Most of centrin in animal cells is not centrosome-associated and centrosomal centrin is confined to the distal lumen of centrioles, *J. Cell Sci. 109*, 3089−3102.
16. Araki, M., Masutani, C., Takemura, M., Uchida, A., Sugasawa, K., Kondoh, J., Ohkuma, Y., and Hanaoka, F. (2001) Centrosome protein centrin 2/caltractin 1 is part of the xeroderma pigmentosum group C complex that initiates global genome nucleotide excision repair, *J. Biol. Chem. 276*, 18665−18672.
17. Fischer, T., Rodriguez-Navarro, S., Pereira, G., Racz, A., Schiebel, E., and Hurt, E. (2004) Yeast centrin Cdc31 is linked to the nuclear mRNA export machinery, *Nat. Cell Biol. 6*, 840−848.
18. Giessl, A., Pulvermuller, A., Trojan, P., Park, J. H., Choe, H.-W., Ernst, O. P., Hofmann, K. P., and Wolfrum, U. (2004) Differential expression and interaction with the visual G-protein transducin of centrin isoforms in mammalian photoreceptor cells, *J. Biol. Chem. 279*, 51472−51481.
19. Gonda, K., Yoshida, A., Oami, K., and Takahashi, M. (2004) Centrin is essential for the activity of the ciliary reversal-coupled voltage-gated Ca^{2+} channels, *Biochem. Biophys. Res. Commun. 323*, 891−897.
20. Tourbez, M., Firanescu, C., Yang, A., Unipan, L., Duchambon, P., Blouquit, Y., and Craescu, C. T. (2004) Calcium-dependent self-assembly of human centrin 2, *J. Biol. Chem. 279*, 47672−47680.
21. Yang, A., Miron, S., Duchambon, P., Assairi, L., Blouquit, Y., and Craescu, C. T. (2006) The N-terminal domain of human centrin 2 has a closed structure, binds calcium with a very low affinity, and plays a role in the protein self-assembly, *Biochemistry 45*, 880−889.
22. Volker, M., Monè, M. J., Karmakar, P., van Hoffen, A., Schul, W., Vermeulen, W., Hoeijmakers, J. H. J., van Driel, R., van Zeeland, A. A., and Mullenders, L. H. F. (2001) Sequential assembly of the nucleotide excision repair factors *in vivo*, *Mol. Cell 8*, 213−224.
23. Riedl, T., Hanaoka, F., and Egly, J.-M. (2003) The comings and goings of nucleotide excision repair factors on damaged DNA, *EMBO J. 22*, 5293−5303.
24. Nishi, R., Okuda, Y., Watanabe, E., Mori, T., Iwai, S., Masutani, C., Sugasawa, K., and Hanaoka, F. (2005) Centrin 2 stimulates nucleotide excision repair by interacting with xeroderma pigmentosum group C protein, *Mol. Cell. Biol. 25*, 5664−5674.
25. Molinier, J., Ramos, C., Fritsch, O., and Hohn, B. (2004) CENTRIN2 modulates homologous recombination and nucleotide excision repair in *Arabidopsis*, *Plant Cell 16*, 1633−1643.
26. Popescu, A., Miron, S., Blouquit, Y., Duchambon, P., and Craescu, C. T. (2003) Xeroderma pigmentosum group C protein possesses a high affinity binding site for human centrin 2 and calmodulin, *J. Biol. Chem. 278*, 40252−40261.
27. Wüthrich, K. (1986) *NMR of Proteins and Nucleic Acids*, Wiley, New York.
28. Cavanagh, J., Fairbrother, W., J., Palmer, A. G., III, and Skelton, N., J. (1996) *Protein NMR Spectroscopy. Principles and Practice*, Academic Press, San Diego, CA.
29. Wishart, D. S., Bigam, C. G., Yao, J., Abildgaard, F., Dyson, H. J., Oldfield, E., Markley, J. L., and Sykes, B. D. (1995) ^{1}H, ^{13}C,

and ^{15}N chemical shift referencing in biomolecular NMR, *J. Biomol. NMR 6*, 135−140.
30. Brooks, B. R., Bruccoleri, R. E., Olafson, B. D., States, D. J., Swaminathan, S., and Karplus, M. (1983) CHARMM: A program for macromolecular energy, minimization, and dynamics calculations, *J. Comput. Chem. 4*, 187−217.
31. MacKerell, A. D., Jr., Bashford, D., Bellott, M., Dunbrack, R. L., Jr., Evanseck, J. D., Field, M. J., Fischer, S., Gao, J., Guo, H., Ha, S., Joseph-McCarthy, D., Kuchnir, L., Kuczera, K., Lau, F. T. K., Mattos, C., Michnick, S., Ngo, T., Nguyen, D. T., Prodhom, B., Reiher, W. E., III, Roux, B., Schlenkrich, M., Smith, J. C., Stote, R., Straub, J., Watanabe, M., Wiórkiewicz-Kuczera, J., Yin, D., and Karplus, M. (1998) All-atom empirical potential for molecular modeling and dynamics studies of protein, *J. Phys. Chem. B 102*, 3586−3616.
32. Chou, J. J., Li, S., Klee, C. B., and Bax, A. (2001) Solution structure of Ca^{2+}-calmodulin reveals flexible hand-like properties of its domains, *Nat. Struct. Biol. 8*, 990−997.
33. Ikura, M., Clore, G. M., Gronenborn, A. M., Zhu, G., Klee, C. B., and Bax, A. (1992) Solution structure of a calmodulin−target peptide complex by multidimensional NMR, *Science 256*, 632−638.
34. Meador, W. E., Means, A. R., and Quiocho, F. A. (1992) Target enzyme recognition by calmodulin: 2.4 Å structure of a calmodulin−peptide complex, *Science 257*, 1251−1255.
35. Meador, W. E., Means, A. R., and Quiocho, F. A. (1993) Modulation of calmodulin plasticity in molecular recognition on the basis of X-ray structures, *Science 262*, 1718−1721.
36. Elshorst, B., Hennig, M., Försterling, H., Diener, A., Maurer, M., Schulte, P., Schwalbe, H., Griesinger, C., Krebs, J., Schmid, H., Vorherr, T., and Carafoli, E. (1999) NMR solution structure of a complex of calmodulin with a binding peptide of the Ca^{2+} pump, *Biochemistry 38*, 12320−12332.
37. Bertini, I., Del Bianco, C., Gelis, I., Katsaros, N., Luchinat, C., Parigi, G., Peana, M., Provenzani, A., and Zoroddu, M. A. (2004) Experimentally exploring the conformational space sampled by domain reorientation in calmodulin, *Proc. Natl. Acad. Sci. U.S.A. 101*, 6841−6846.
38. Grabarek, Z. (2005) Structure of a trapped intermediate of calmodulin: Calcium regulation of EF-hand proteins from a new perspective, *J. Mol. Biol. 346*, 1351−1366.
39. Forsén, S., and Linse, S. (1995) Cooperativity: Over the hill, *Trends Biochem. Sci. 20*, 495−497.
40. Linse, S., Helmersson, A., and Forsen, S. (1991) Calcium binding to calmodulin and its globular domains, *J. Biol. Chem. 266*, 8050−8054.
41. Linse, S., Johansson, C., Brodin, P., Grundstrom, T., Drakenberg, T., and Forsen, S. (1991) Electrostatic contributions to the binding of Ca^{2+} in calbindin D_{9k}, *Biochemistry 30*, 154−162.
42. Engelborghs, Y., Mertens, K., Willaert, K., Luan-Rilliet, Y., and Cox, J., A. (1990) Kinetics of conformational changes in *Nereis* sarcoplasmic calcium-binding protein upon binding of divalent ions, *J. Biol. Chem. 265*, 18809−18815.
43. Yazawa, M., Vorherr, T., James, P., Carafoli, E., and Yagi, K. (1992) Binding of calcium by calmodulin: Influence of the calmodulin binding domain of the plasma membrane calcium pump, *Biochemistry 31*, 3171−3176.
44. Hoeflich, K. P., and Ikura, M. (2002) Calmodulin in action: Diversity in target recognition and activation mechanisms, *Cell 108*, 739−742.
45. Vetter, S. W., and Leclerc, E. (2003) Novel aspects of calmodulin target recognition and activation, *Eur. J. Biochem. 270*, 404−414.
46. Babu, Y. S., Bugg, C. E., and Cook, W. J. (1988) Structure of calmodulin refined at 2.2 Å resolution, *J. Mol. Biol. 204*, 191−204.
47. Yap, K. L., Kim, J., Truong, K., Sherman, M., Youan, T., and Ikura, M. (2001) Calmodulin target database, *J. Struct. Funct. Genomics 1*, 8−14.
48. Hu, H., and Chazin, W. J. (2003) Unique features in the C-terminal domain provide caltractin with target specificity, *J. Mol. Biol. 330*, 473−484.
49. Brokx, R. D., Lopez, M. M., Vogel, H. J., and Makhatadze, G. I. (2001) Energetics of target peptide binding by calmodulin reveals different modes of binding, *J. Biol. Chem. 276*, 14083−14091.
50. Kurokawa, H., Osawa, M., Kurihara, H., Katayama, N., Tokumitsu, H., Swindells, M. B., Kainosho, M., and Ikura, M. (2001) Target-induced conformational association of calmodulin revealed by the crystal structure of a complex with nematode Ca^{2+}/calmodulin-dependent kinase kinase peptide, *J. Mol. Biol. 312*, 59−68.
51. Ivanovska, I., and Rose, M. D. (2001) Fine structure analysis of the yeast centrin, Cdc31p, identifies residues specific for cell morphology and spindle pole body duplication, *Genetics 157*, 503−518.
52. Spolar, R. S., and Record, M. T., Jr. (1994) Coupling of local folding to site-specific binding of proteins to DNA, *Science 263*, 777−784.
53. Kalodimos, C. G., Boelens, R., and Kaptein, R. (2004) Toward an integrated model of protein−DNA recognition as inferred from NMR studies on the Lac repressor system, *Chem. Rev. 104*, 3567−3586.
54. Uchida, A., Sugasawa, K., Masutani, C., Dohmae, N., Araki, M., Yokoi, M., Ohkuma, Y., and Hanaoka, F. (2002) The carboxy-terminal domain of XPC protein plays a crucial role in nucleotide excision repair trough interactions with transcription factor IIH, *DNA Repair 1*, 449−461.
55. Osawa, M., Tokumitsu, H., Swindells, M. B., Kurihara, H., Orita, M., Shibanuma, T., Furuya, T., and Ikura, M. (1999) A novel target recognition revealed by calmodulin in complex with Ca^{2+}-calmodulin-dependent kinase kinase, *Nat. Struct. Biol. 6*, 819−824.
56. Clapperton, J. A., Martin, S. R., Smerdon, S. J., Gamblin, S. J., and Bayley, P. M. (2002) Structure of the complex of calmodulin with target sequence of calmodulin-dependent protein kinase I: Studies of the kinase activation mechanism, *Biochemistry 41*, 14669−14679.
57. Kraulis, P. (1991) MOLSCRIPT: A program to produce both detailed and schematic plots of protein structures, *J. Appl. Crystallogr. 24*, 946−950.
58. Merritt, E. A., and Bacon, D., J. (1977) Raster3D-photorealistic molecular graphics, *Methods Enzymol. 277*, 505−524.

BI0524868